Journal of Wind Engineering & Industrial Aerodynamics 198 (2020) 104100

Contents lists available at ScienceDirect

Journal of Wind Engineering & Industrial Aerodynamics

journal homepage: www.elsevier.com/locate/jweia

VIV regimes and simplified solutions by the spectral model description

L.C. Pagnini, G. Piccardo *, G. Solari

Department of Civil, Chemical and Environmental Engineering – DICCA, Polytechnic School, University of Genoa, Via Montallegro 1, 16145, Genoa, Italy

ARTICLE INFO

Keywords:
Vortex-induced vibrations (VIVs)
VIV spectral model
VIV regimes
Closed-form solutions

ABSTRACT

The present paper discusses technical aspects of the vortex-induced vibrations (VIVs) of structures excited by the wind in the framework of the spectral model, which is applied by many codes and guidelines for civil engineering verifications. Quantitative thresholds related to Scruton number domains, where the structural response can be considered in "forced vibration" or "lock-in" regime, are proposed. In this way, the type of VIV response and its evaluation can be assessed with simple calculations that use the parameters already present in codes and guidelines. An analytical solution of the original model allows straightforward evaluations inclusive of operative criteria to properly consider structural and flow conditions concerning the coefficients governing the VIV response in the spectral description, leaving out some assumptions that are commonly adopted. Extensive numerical applications, limited here to circular cylinders and including a real full-scale chimney, allow to identify the most significant parameters of the model and the criticalities connected with their choice.

1. Introduction

Vortex-Induced Vibrations (VIVs) represent one of the most important issues concerning wind excited slender structures and elements as well as bluff bodies in air and water (e.g., Solari, 2019). Although its great significance, the engineering description of this phenomenon mainly comes from the experimental evidence and uses empirical models.

Key parameters for VIVs are the Strouhal number, $St = b\ n/\ U$ and the Scruton number, $Sc = 4\pi m_e \xi/\rho b^2$, being U the mean flow velocity, n the vortex shedding frequency (set equal to a structural frequency in critical conditions), ρ the density of the air, b the crosswind characteristic dimension of the bluff body, ξ the structural damping ratio, m_e the mass per unit length (more in general the equivalent mass per unit length related to a critical mode). The Strouhal number determines the frequency of vortex shedding from the structure and, therefore, rules the critical velocity at resonant conditions. It is related to the cross-section shape and, in the case of structures with rounded surfaces, it is Reynolds number dependent, since the Reynolds number directly rules the vortex shedding topology. The Scruton number governs the synchronization region at lock-in. At high Sc values, a structure undergoes low amplitude linear vibrations in random forcing regime. Conversely, at low Sc, non-linear resonant vibrations arise in lock-in conditions. When dealing with structural verifications this is the discriminating quantity that allows either to exclude or to highlight possible critical VIVs. However, the scientific literature on this topic does not supply specific quantitative limits in terms of Scruton number; technical applications refer to high enough values for excluding synchronous vibrations (e.g., $Sc > 30$ for circular cross-sections according to CNR, 2008).

According to Païdoussis et al. (2011), the description of crosswind VIVs comes from three families of phenomenological models of increasing complexity. *Forced system models* consider a cylinder excited by a force independent from its motion, therefore only depending on time (e.g., Ruscheweyh, 1994; Blevins, 2001). In *fluid-elastic system models*, the vortex-induced force also depends on the cylinder motion through an equivalent fluid-structure interactive term (e.g., Vickery and Basu, 1983a; Goswami et al., 1993). *Coupled system models* are a further evolution that considers explicitly the interaction with the wake dynamics; in case of crosswind VIV they are described by two degree of freedom systems, including the dependence on both the cylinder motion and the wake oscillation (e.g., Hartlen and Currie, 1970; Skop and Griffin, 1973; Tamura and Matsui, 1979; Facchinetti et al., 2004). At present, coupled system models are quite diffused in hydrodynamics whereas they have limited technical applications in aerodynamics (e.g., Farshidianfar and Zanganeh, 2010; Violette et al., 2010).

Dealing with wind engineering verifications, two calculation procedures are commonly used, respectively of forced and fluid-elastic type (e.g., EN, 1991-1-4, 2005). The first method, referred to as the *harmonic model*, was proposed by Ruscheweyh (1994) who supplied a heuristic vortex-induced force based on the correlation length parameter, which increases with increasing vibration amplitude. The second method,

* Corresponding author.
E-mail address: giuseppe.piccardo@unige.it (G. Piccardo).

https://doi.org/10.1016/j.jweia.2020.104100
Received 23 July 2019; Received in revised form 14 January 2020; Accepted 14 January 2020
Available online 31 January 2020

referred to as the *spectral model*, was proposed by Vickery and Basu (1983a) who supplied an analytical expression for the equivalent aerodynamic damping, derived from a modified van der Pol oscillator, accounting for the intrinsic non-linearity of the problem and its self-limiting features. The method proposed by ESDU 96030 (1998) can be considered as a hybrid of the two previously described approaches (Holmes, 1998). It adopts a random excitation model, similar to the spectral model, at low amplitudes and assumes a harmonic model at large amplitude. All these formulations lead to evaluations that may involve considerable uncertainties compared to measured data (e.g., ESDU 96030; Hansen, 1999; Kawecki and Żurański, 2007). The spectral formulation is commonly considered more sound and more prudential. Moreover, it is considered more reliable at sufficiently high Scruton numbers, when the response tends to be in the so-called "forced vibration" regime.

Within the fluid-elastic system framework, the Vickery and Basu model marked a turning point in engineering evaluations, providing a bridge between technical needs, such as considering spectral density models of excitation and a fluctuating lift coefficient, and analytical requirements, such as modelling a linearized aerodynamic damping deriving from a van der Pol approach. In its original formulation, the problem was derived in the context of linear random dynamics, involving a challenging numerical solution. Dyrbye and Hansen (1997) supplied technical developments that allow dealing with line integrals rather than with double integrals of the spectrum function. The complete analytical solution still remains not easy to use and, for this reason, it is seldom applied (e.g., Verboom and van Koten, 2010; Pagnini and Piccardo, 2017). The reworking of the spectral model in terms of simplified analytical coefficients (e.g., Hansen, 1999, 2007) makes it possible including this procedure into codes and guidelines.

However, engineering applications often adopt extreme simplifications, the reliability of which has not been adequately explored yet. Contradictory outcomes can be found compared to the experimental results (e.g., Hansen, 1999; Ruscheweyh and Sedlaceck, 1988). Moreover, at the best of the authors' knowledge, there are no extended comparisons between complete and approximate solutions. Especially, there are no broad-range analyses of the sensitivity to the model parameters whose uncertainties are the greatest hindrance to the analytical prediction of VIVs. At this purpose, Pagnini and Piccardo (2017) highlighted the fundamental role of the limiting amplitude, in both transition and lock-in regime, in order to find realistic value of the VIV maximum amplitude. On the other hand, Basu and Vickery (1983) explicitly stated that the proposed "response calculations for realistic, stable structures are likely to be fairly insensitive" to this quantity, as they presume that large amplitudes "would almost certainly be unacceptable in working conditions". These sentences highlight that, at very small Scruton numbers, the model can lead to unreliable response estimates, since it has not been thought nor has it never been calibrated (at least until today) for such conditions.

Starting from these premises, and working in the frame of the Vickery and Basu model in its original spirit, the present paper intends to provide calculation developments suitable for engineering applications, maintaining the rigor of the initial formulation, as well as the explicit dependence on the different parameters. In this context, the paper aims to define an analytical method for assessing the thresholds of VIV structural sensitivity (e.g., forced or lock-in conditions), which are usually chosen in a heuristic way by researchers, practitioners and codes. Section 2 recalls the classic model by Vickery and Basu, highlighting its main terms and their derivation. With respect to the original model, a more general expression of the limiting amplitude is used including the modal deformation. Section 3 investigates the conditions where the structural response can be considered belonging to "forced vibration" or "lock-in" regime. Suitable domains for direct use in calculations are defined, as well as approximated closed-form solutions, suitable to distinguish the two behavior regimes. Section 4 derives closed form solutions of the wake excitation parameters for the VIV estimate. Recalling well established simplified procedures for the evaluation of the wind response of slender structures, the original formulation is developed according to different approximation levels. Section 5 develops numerical evaluations in line with European code provisions, investigating the main quantities on which the solution depends with reference to circular cylinders; comparisons with in-field measures are carried out over a full-scale chimney. Section 6 draws the main conclusions and provides some prospects.

2. VIV response

Let us consider a slender structural element of length L and cross section size b immersed in a wind field of direction X and mean flow intensity U (Fig. 1). It is inclined φ with respect to the vertical axis Z and variously supported at its end. Let x, y, z be a Cartesian local reference system with origin in O at height h above the ground; z coincides with the structural axis, x is aligned with the mean wind direction. The element is subjected to a vortex-induced force $f(z,t)$ varying over time t and space z. The continuum equation of motion in the cross-wind direction is:

$$\mu(z)\frac{\partial^2 y(z,t)}{\partial t^2}+\frac{\partial}{\partial t}\mathscr{D}[y(z,t)]+\mathscr{R}[y(z,t)]=f(z,t) \tag{1}$$

where $y(z,t)$ is the cross-wind displacement, $\mu(z)$ is the beam mass per unit length, $\mathscr{D}$, $\mathscr{R}$ are the damping and stiffness operators, respectively. Assuming a lack of correlation between the vortex-shedding forces induced on the stationary cylinder and the motion-induced actions (e.g., Vickery and Basu, 1983a), the force $f(z,t)$ can be expressed as the sum of two distinct terms, respectively related to the "stationary" vortex shedding and to the motion-induced forces:

$$f(z,t)=\frac{1}{2}\rho U^2(z)b(z)c_{ls}(z,t)+\mathscr{F}[y(z,t),Re]\ \dot{y}(z,t) \tag{2}$$

The former term is governed by a space- and time-dependent lift coefficient c_{ls} (e.g., Vickery and Basu, 1983a; Dyrbye and Hansen, 1997). The latter identifies the motion-induced forces through a suitable force operator $\mathscr{F}$, which is a nonlinear function of parameters of both the fluid (e.g., the Reynold number Re) and the structure (e.g., the structural displacement y and its derivatives). The influence of turbulence is implicit in the formulation (e.g., it influences the values of aerodynamic and aeroelastic coefficients) but it does not appear explicitly in the equations, as usual in the literature (e.g., Blevins, 2001). Scruton and co-workers (e.g., Scruton and Flint, 1964) proposed expressing the aerodynamic lift force per unit length as the sum of a displacement-dependent term and a velocity-dependent term. The former, which is representative of the aerodynamic force in phase with the motion (and, therefore, modifies the structural stiffness) is usually negligible compared with the structure elastic force (Vickery and Basu, 1983a).

Applying the modal transformation, $y(z,t)=\sum_k \psi_k(z)a_k(t)$, a_k being the principal k-th modal amplitude related to the cross-wind motion and ψ_k the corresponding k-th modal shape, under the hypothesis of classical

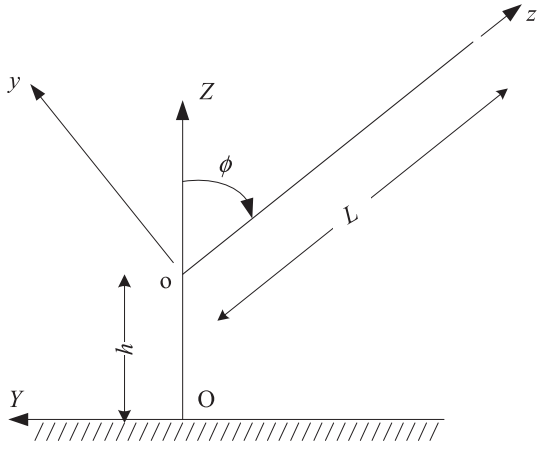

Fig. 1. Structural model (X entering direction).

damping, Eq. (1) becomes:

$$\ddot{a}_j(t) + 2\left(2\pi n_j\right)\,\xi_j^m\,\dot{a}_j(t) + \left(2\pi n_j\right)^2 a_j(t) = \frac{\rho}{2m_j}\int_0^L U^2(z)c_{ls}(z,t)b(z)\psi_j(z)dz + \\ + \frac{1}{m_j}\sum_k\left(\int_0^L \mathscr{F}_k(z,t,Re)\;\psi_k(z)\;\psi_j(z)dz\right)\;\dot{a}_k(t) \tag{3}$$

where n_j is the j-th modal frequency, ξ_j^m is the j-th modal mechanical damping ratio, $m_j = \int_0^L \mu(z)\psi_j^2(z)\;dz$ is the modal mass of mode j, $\mathscr{F}_k$ is the k-th modal counterpart of the continuous force operator $\mathscr{F}$.

Using the spectral model developed in the framework of linear random dynamics, following Basu and Vickery (1983) and Vickery and Basu (1983a), three assumptions are made: a) the forcing "stationary" term is described in the frequency domain by the r.m.s. lift coefficient, c_{ls}^{rms}, through the power spectral density function of c_{ls} (z,t) in the classic form proposed by Vickery and Clark (1972); (b) the motion-induced excitation concerns a single mode at a time, i.e. $\mathscr{F}_k = 0$ for $k \neq j$ in Eq. (3), then the model is able to include fluid-structure interaction for (sufficiently) well-separated modes only; (c) the physical nonlinearity of the motion-induced term $\mathscr{F}_k$ is considered in a statistical form only, through a suitable ratio of r.m.s. cross-wind displacements. Therefore, the j-th modal force operator can be expressed as:

$$\mathscr{F}_j(z,Re) = 2\left(2\pi n_j\right)\rho\;\;b^2(z)\;\;K_{a0}(z,Re)\left[1-\left(\frac{\sigma_j(z)}{\sigma_{j,L}}\right)^2\right] \tag{4}$$

where σ_j is the r.m.s. Displacement related to the mode j and $\sigma_{j,L}$ is the limiting r.m.s. amplitude of VIV displacements, being the phenomenon self-limited in nature. K_{a0} is the aerodynamic damping parameter for small oscillation amplitudes (i.e., when $\sigma_j \to 0$); its values and shape are strongly influenced by the longitudinal turbulence intensity I_u (e.g., Verboom and van Koten, 2010). On the other hand, the dependence on the turbulence integral length scale is not included; this parameter seems to have a modest influence on VIV-induced r.m.s. displacements in both low-amplitude and high-amplitude regimes (Acebedo et al., 2016; Daniels et al., 2016; Vickery and Basu, 1983a).

Basu and Vickery (1983) express the limiting amplitude of the full scale element as a function of the characteristic size (e.g., the diameter of a circular cross-section), $\sigma_{j,L}(z) = b(z)/\kappa$, $1/\kappa$ being a suitable fraction of b. This choice appears, however, more suitable for a bi-dimensional description, rather than for a full-scale modelling, because it does not account for the geometric boundary conditions of the element (for instance, it does not provide any variation along z in the case of a structure with a constant diameter). In the spirit of a real full-scale description, the limiting amplitude is herein modulated through the j-th modal shape under consideration, thus enhancing the model with the correct kinematic conditions:

$$\sigma_{j,L}(z) = \frac{\psi_j(z)}{\psi_j(\widehat{z})}\,\frac{b_{ref}}{\kappa} \tag{5}$$

where $\widehat{z}$ identifies the position of the maximum modal displacement (e.g., the tip of a cantilever or the mid-span of a simply-supported beam, concerning their first modes) and b_{ref} is a reference size. The reference size can be assumed equal to $b(\widehat{z})$ or to any other value representative for VIV calculations (e.g., the top one-third diameter for chimneys excited in the first mode, Vickery and Basu, 1983b).

With the previous assumptions, the equation of motion for the generic j-th mode can be expressed as:

$$\ddot{a}_j(t) + 2\left(2\pi n_j\right)\,\xi_j\dot{a}_j + \left(2\pi n_j\right)^2 a_j(t) = \frac{1}{m_j}\int_0^L f_l\;(z,t)\;\;\psi_j(z)dz \tag{6}$$

where

$$f_l\;(z,t) = \frac{1}{2}\rho U^2\;(z)b(z)c_{ls}\;(z,t) \tag{7}$$

ξ_j is the damping coefficient accounting for both the mechanical ξ_j^m and the aerodynamic ξ_j^a contribution:

$$\xi_j = \xi_j^m + \xi_j^a,\; \xi_j^a = -\frac{\rho b_{ref}^2}{m_{ej}}c_1^a\left[1-\left(\frac{\psi_j(\widehat{z})\kappa\sigma_{aj}}{b_{ref}}\right)^2\right] \tag{8}$$

being c_1^a a dimensionless quantity related to possible variations of the aerodynamic damping along the element span:

$$c_1^a = \frac{\int_0^L \gamma^2(z)\;\;K_{a0}(z,Re)\psi_j^2(z)dz}{\int_0^L \psi_j^2(z)dz},\gamma(z) = b(z)\Big/ b_{ref} \tag{9}$$

and m_{ej} is the j-th equivalent mass per unit length:

$$m_{ej} = \frac{m_j}{\int_0^L \psi_j^2(z)dz} \tag{10}$$

The coefficient ξ_j can be considered as an equivalent damping ratio able to approximate the nonlinearity induced by the aerodynamic interaction; the expression of the equivalent aerodynamic contribution, Eq. $(8)_2$, can also be obtained using statistical linearization techniques (e.g., Chen, 2014).

In the frequency domain, the standard deviation of the principal coordinate, σ_{aj}, is obtained by:

$$\sigma_{aj}^2 = \int_0^\infty \left|H_j(n)\right|^2 S_{Q_j}(n,z)\;\;dn \tag{11}$$

where $H_j(n)$ is the j-th frequency response function and S_{Q_j} is the cross-power spectral density function of the wake excitation related to mode j:

$$S_{Q_j}(n) = \int_0^L\int_0^L f_l\;(z)f_l\;(z')S_{ss}^*(z,z',n)\psi_j(z)\psi_j(z')dzdz' \tag{12}$$

S_{ss}^* being the cross-power spectral density function (CPSDF):

$$S_{ss}^*(z,z',n) = \sqrt{S_{ss}^*(z,n)S_{ss}^*(z',n)}Coh_{ss}(z,z',n) \tag{13}$$

and Coh_{ss} the coherence function.

Neglecting the quasi-static response and introducing the dimensionless quantity $a_L = \sigma_{aj,L}/b_{ref}$, the dimensionless response standard deviation $\tilde{\sigma}_{aj} = \sigma_{aj}/b_{ref}$ can be expressed as:

$$\tilde{\sigma}_{aj} = \frac{c}{\sqrt{\frac{Sc}{4\pi} - c_1^a\left[1-\left(\frac{\tilde{\sigma}_{aj}}{a_L}\right)^2\right]}} \tag{14}$$

being:

$$c = \sqrt{\frac{m_{ej}}{\rho b_{ref}^2}c_f^a} \tag{15}$$

$$c_f^a = \frac{\pi n_j}{4m_j^2\left(2\pi n_j\right)^4}\left(\frac{\rho c_{ls,ref}^{rms}}{2}\right)^2\int_0^L \\ \times\int_0^L U^2(z)U^2(z')\;\gamma_s^*(z)\;\gamma_s^*(z')\;\psi_j(z)\;\psi_j(z')\;S_{ss}^*\left(z,z';n_j\right)\;dz\,dz' \tag{16}$$

$$\gamma_s^*(z) = \gamma(z)\frac{c_{ls}^{rms}(z)}{c_{ls,ref}^{rms}} \tag{17}$$

where c, c_f^a, γ_s^* are suitable dimensionless quantities, c_{ls}^{rms} is the r.m.s. value of c_{ls} and $c_{ls,ref}^{rms}$ is its reference value; the Scruton number is then evaluated as $Sc = 4\pi\xi_j^m m_{ej}/\rho b_{ref}^2$. Eq. (14) is formally coincident with the expression provided by Vickery and Basu (1983a, Eq. (31)), generalized with the new, more consistent definition of limiting amplitude.

The implicit expression (14) can be solved in terms of $\tilde{\sigma}_{aj}$ (e.g., Dyrbye and Hansen, 1997):

$$\tilde{\sigma}_{aj} = \sqrt{c_{1F} + \sqrt{c_{1F}^2 + c_{2F}}} \tag{18}$$

where c_{1F} and c_{2F} are the dimensionless quantities:

$$c_{1F} = \frac{a_L^2}{2}\left(1 - \frac{Sc}{4\pi c_1^a}\right) \tag{19}$$

$$c_{2F} = \frac{c^2}{c_1^a}a_L^2 \tag{20}$$

3. Quantitative characterization of the VIV domains

The wake-excited response model supplied by Vickery and Basu for a cylinder in two-dimensional conditions (Vickery and Basu, 1983a, Eq. (31)) can be expressed in approximate form for two different domains, depending on the VIV regime. The former applies in the low-amplitude case of a linear system subjected to random forcing, when the structural damping parameter is much higher than the aerodynamic damping one (Eq. (32a) of the cited paper). The latter applies for nonlinear large-amplitude or in lock-in situation, when the structural damping parameter is much smaller than the aerodynamic one and the amplitude is virtually independent of external forcing (Eq. (32b) of the cited paper). Working in the same spirit, the implicit full-scale solution, Eq. (14), is reduced to the following approximate expressions in terms of Scruton number:

$$\tilde{\sigma}_{aj}^f = \frac{c}{\sqrt{\frac{Sc}{4\pi} - c_1^a}}, Sc \gg 4\pi c_1^a \tag{21}$$

$$\tilde{\sigma}_{aj}^{nl} = a_L\sqrt{1 - \frac{Sc}{4\pi c_1^a}}, Sc \ll 4\pi c_1^a \tag{22}$$

where $\tilde{\sigma}_{aj}^f$, $\tilde{\sigma}_{aj}^{nl}$ are, respectively, the dimensionless response in the "forced vibration" and in the "lock-in" regime.

In line with Fig. 9 by Vickery and Basu (1983a), Fig. 2 represents the wake-excited response of the world-renowned wind-tunnel tests performed by Wootton (1969) on a circular chimney model. The diagram shows the exact solution (gray line) given by Eq. (14), assuming the same values of the parameters used by Vickery and Basu for this case study. It also reports the approximate solution in forced (dotted line) and lock-in (dashed line) conditions, supplied by Equations (21) and (22), respectively.

Fig. 2 highlights the accuracy of the approximate solutions that cover almost the whole domain in terms of Scruton number. In particular, Eq. (21) approaches Eq. (14) from upward, by providing conservative values, whereas Eq. (22) approaches Eq. (14) from downward. At present, however, no criterion is available to quantify the domain of validity of such simplified relationships.

This aspect represents a major shortcoming from the scientific and technical viewpoint. Many researchers, practitioners and code provisions frequently refer to heuristic thresholds in terms of Scruton number, below which structures are highly vulnerable to lock-in conditions.

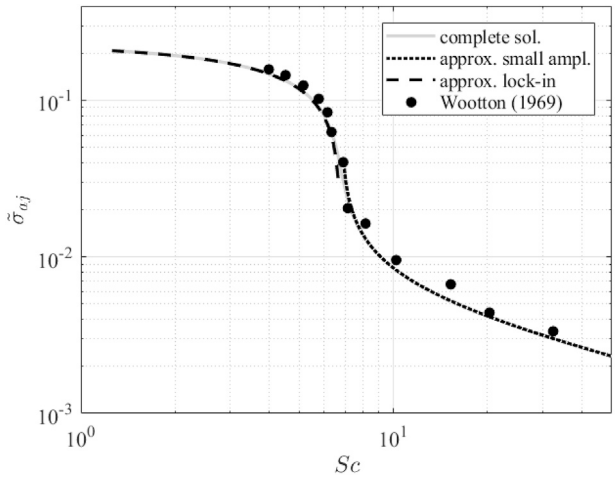

Fig. 2. Reworking of Fig. 9 by Vickery and Basu (1983a) setting $c = 0.0043$, $a_L = 0.23$ and $c_{1a} = K_{a0} = 0.54$ as in the cited paper.

However, there is no robust framework that may justify such thresholds. A reliable method would be extremely useful (especially in the pre-design phase) to recognize the behavior of structures with regard to vortex shedding and lock-in phenomena. This is exactly the goal of the present Section.

To identify the thresholds, Eqs. (21) and (22) may be expressed in terms of the coefficients c_{1F} and c_{2F} appearing in the explicit form solution, Eq. (18). It follows (see also Verboom and van Koten, 2010):

$$\tilde{\sigma}_{aj}^f = \sqrt{-\frac{1}{2}\frac{c_{2F}}{c_{1F}}}, \quad c_{1F} \ll 0 \tag{23}$$

$$\tilde{\sigma}_{aj}^{nl} = \sqrt{2c_{1F}}, \quad c_{1F} \gg 0 \tag{24}$$

It should be noted that c_{2F}, Eq. (20), always has a positive sign since the aerodynamic coefficient c_1^a is ruled by the aerodynamic damping parameter K_{a0}, which assumes positive values in the critical range (e.g., Pagnini and Piccardo, 2017). For the same case study, Fig. 3 clarifies the accuracy of Eqs. (23) and (24), giving the representation of the previous diagram in terms of c_{1F} (which is a function of the Scruton number) and c_{2F} (which is fixed by the parameter assumptions). The approximate solution $\tilde{\sigma}_{aj}^f$ matches the exact one for small enough values of c_{1F}, providing conservative results; it grows suddenly in the vicinity of $c_{1F} = 0$ approaching infinity. The approximate solution $\tilde{\sigma}_{aj}^{nl}$ matches the exact

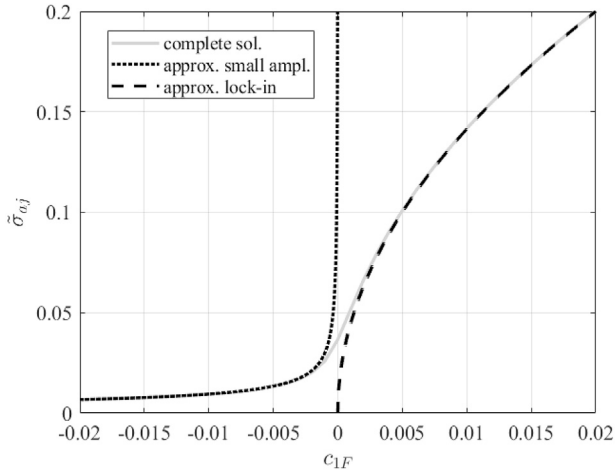

Fig. 3. Exact and approximated solutions for the Wootton case study ($c_{2F} \cong 1.81 \cdot 10^{-6}$).

one for large enough values of c_{1F}; it approaches zero as c_{1F} approaches zero. The "transition" regime arises around $c_{1F} = 0$.

Fig. 3 highlights that, for c_{1F} little greater than 0, the approximated lock-in solution $\tilde{\sigma}_{aj}^{nl}$ holds, whereas, for c_{1F} little smaller than 0, the approximated small amplitude solution $\tilde{\sigma}_{aj}^{f}$ takes validity. From Eq. (18) it comes the possibility of expressing the response based on a single parameter; c_{2F}, which is always positive, seems the suitable choice. In a purely empirical manner, a quantification of the validity domain for the "forced vibration" regime can be obtained considering the negative value $c_{1F} = -2\sqrt{c_{2F}}$. In this specific case, the exact (18) and the approximate (23) solutions lead to, respectively:

$$\tilde{\sigma}_{aj} = \sqrt{\sqrt{5}-2}\ \sqrt[4]{c_{2F}};\quad \tilde{\sigma}_{aj}^{f} = \frac{1}{2}\sqrt[4]{c_{2F}} \tag{25}$$

where $\tilde{\sigma}_{aj}^{f}$ approximates $\tilde{\sigma}_{aj}$ with a positive error of about 3%. Therefore, if $c_{1F} \le -2\sqrt{c_{2F}}$, Eq. (23) supplies the solution with a (positive) error less than 3% with respect to Eq. (18). In terms of Scruton number, from Eq. (19), the approximation holds for $Sc \ge 4\pi c_1^a[1 + 4\sqrt{c_{2F}}/a_L^2]$, which corresponds to the threshold $Sc \ge 7.5$ for the Wootton case study.

Similarly, a quantification of the validity domain for the "lock-in" regime can be obtained considering the positive value $c_{1F} = \sqrt{5c_{2F}}$. In this specific case, it reads:

$$\tilde{\sigma}_{aj} = \sqrt[4]{11+2\sqrt{30}}\ \sqrt[4]{c_{2F}};\quad \tilde{\sigma}_{aj}^{nl} = \sqrt{2}\ \sqrt[4]{5}\ \sqrt[4]{c_{2F}} \tag{26}$$

where $\tilde{\sigma}_{aj}^{nl}$ approximates $\tilde{\sigma}_{aj}$ with a negative error of about 3%. Therefore, if $c_{1F} \ge \sqrt{5\ c_{2F}}$, Eq. (24) supplies the solution with a (negative) error less than 3% with respect to Eq. (18). In terms of Scruton number, the approximation holds for $Sc \le 4\pi c_1^a[1 - 2\sqrt{5}\sqrt{c_{2F}}/a_L^2]$, which corresponds to the threshold $Sc \le 6$ for the Wootton case study.

By virtue of these findings, the validity domain of the approximated solutions, that was given in qualitative terms by Eqs. (21)–(23), (24), can be supplied in quantitative terms. Moreover, for sake of simplicity, the two limits can easily be made symmetrical in a conservative way taking the largest value with respect to $4\pi c_1^a$. It derives:

$$\tilde{\sigma}_{aj}^{f} = \frac{c}{\sqrt{\frac{Sc}{4\pi} - c_1^a}} = \sqrt{-\frac{1}{2}\frac{c_{2F}}{c_{1F}}},\quad Sc \ge 4\pi c_1^a\left[1 + \frac{2\sqrt{5}}{a_L^2}\sqrt{c_{2F}}\right] \tag{27}$$

$$\tilde{\sigma}_{aj}^{nl} = a_L\sqrt{1 - \frac{Sc}{4\pi c_1^a}} = \sqrt{2c_{1F}},\quad Sc \le 4\pi c_1^a\left[1 - \frac{2\sqrt{5}}{a_L^2}\sqrt{c_{2F}}\right] \tag{28}$$

with the transition domain lying in between the values:

$$4\pi c_1^a\left(1 - \frac{2\sqrt{5}}{a_L^2}\sqrt{c_{2F}}\right) < Sc < 4\pi c_1^a\left(1 + \frac{2\sqrt{5}}{a_L^2}\sqrt{c_{2F}}\right) \tag{29}$$

Expressed in these terms, the qualitative rules suggested by Vickery and Basu (1983a) and by Verboom and van Koten (2010) for the application of the approximate solutions (i.e., "much smaller than" or "much greater than") become quantitative with an estimate check of the maximum error that is committed in their application. Still referring to the vibrating cylinder investigated by Wootton (1969), Fig. 4 a, b illustrate and clarify this issue, showing the solution behavior in the two regimes and the limit values specified by Eqs. (27)-(29). In this case, the transition domain lies in the range 6 ≤Sc ≤ 7.6, being the quantity $4\pi c_1^a \cong 6.8$.

The evaluation of the domain limits depends on the parameters c_1^a,a_L, c_{2F}. As highlighted by Pagnini and Piccardo (2017), the limiting amplitude a_L is the most uncertain parameter in these calculations. Recalling Eq. (20) that expresses c_{2F}, Eq. (29) points out that the limits are inversely proportional to a_L. Therefore, higher values of a_L lower the boundaries

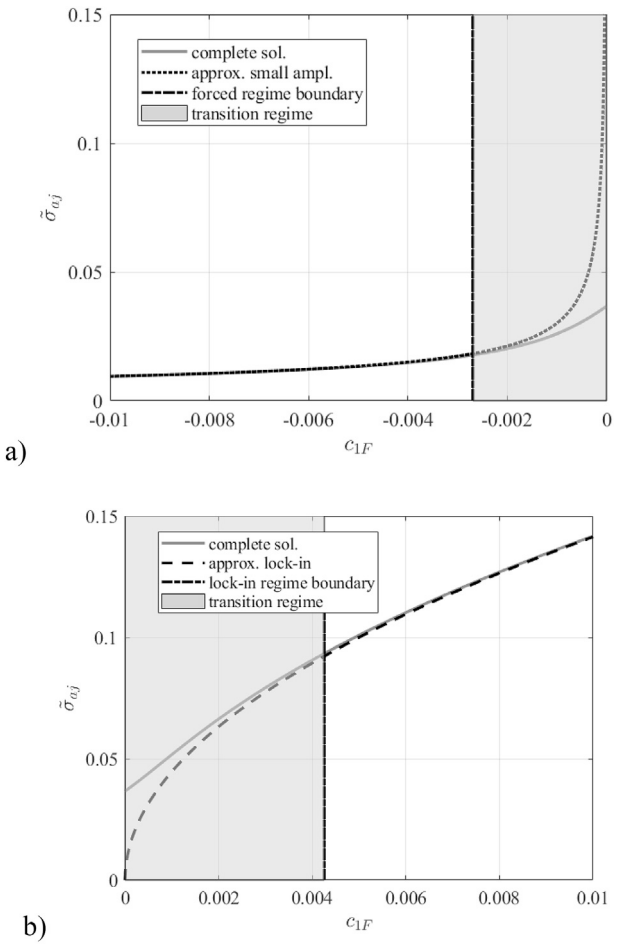

Fig. 4. Domain of validity of the approximate solutions in the forced (a) and lock-in (b) regime for the Wootton case study.

that delimit the two regimes, enlarging the domain of the forced vibration onset and stretching the transition domain. On the other hand, the correct evaluation of c_{2F} is a burdensome task, requiring the computation of the double integral in Eq. (16). In all cases, the domain of the approximate solutions is governed by turbulence intensity I_u and in general by Reynolds number Re, which rule the quantity K_{a0} and therefore c_1^a. Approximate expressions for the coefficients involved will be discussed in the next Section 4. Extensive qualitative and numerical evaluations of VIV domain limits will be developed in Section 5.

It is worth-noting that, whereas the domain limits depends on a_L, the approximate solution for the "forced vibration" regime, given by Eq. (27), is independent from it (since the ratio c_{2F}/c_{1F} does not depend on a_L) and, therefore, it is not affected by the uncertainties in its estimate. Its use is perfectly in the spirit of the Vickery and Basu formulation, as the authors claim that "response calculations for realistic, stable structures are likely to be fairly insensitive to the value assumed for" the limiting amplitude, as mentioned in the Introduction of the paper. On the contrary, the approximate solution for the "lock-in" regime, Eq. (28), is completely governed by the value assumed for a_L.

4. Closed-form expressions for VIV coefficients

With a view to providing operational procedures, it is necessary to obtain straightforward analytical expressions of c_{1F}, c_{2F}, directly derived from the general formulation of the problem (Section 2). In the philosophy of the generalized Equivalent Spectrum Technique (EST; Piccardo and Solari, 1996, 1998, 2000), the following assumptions are adopted: (a) the variation of the aerodynamic and geometrical properties along the

structural axis is neglected, i.e. $\gamma(z) = 1$, Eq. (9), and $\gamma_s^*(z) = 1$, Eq. (17); (b) the mean wind velocity in Eq. (16) is set at a suitable reference coordinate z_{ss}, where the VIV phenomenon is supposed to occur; (c) the structural frequency is set equal to the vortex-shedding frequency, i.e. $n_j = n_s$; (d) consistently with the previous assumptions, the power spectral density functions S_{ss}^* are evaluated at $z = z' = z_{ss}$ with $n = n_j$. The VIV reference coordinate z_{ss} depends on the modal shape under consideration (Fig. 5, Piccardo and Solari, 2000). It can be taken as 0.8 L for modal shapes that reach a maximum at one end (e.g., vertical cantilevers). This choice takes into account that the maximum response occurs at a VIV resonance arising in a position lower than the structural top (e.g., Verboom and van Koten, 2010). It is usually taken at the antinode position in other cases. When the antinodes are more than one (i.e. skew-symmetric or higher modes), the procedure may need to be applied multiple times, considering the resonant phenomenon arising at each antinode.

By virtue of hypotheses (a)-(c), the parameter c_1^a, Eq. (9), simplifies as:

$$c_1^a = K_{a0}(z_{ss}, Re_{ss}) \tag{30}$$

Re_{ss} being the Reynolds number evaluated in critical VIV conditions. Therefore, c_{1F}, Eq. (19), becomes:

$$c_{1F} = \frac{a_L^2}{2}\left[1 - \frac{Sc}{4\pi K_{a0}(z_{ss}, Re_{ss})}\right] \tag{31}$$

which formally coincides with the expression supplied by European codes and guidelines, where K_{a0} appears as a function of Reynolds number only.

As regards c_{2F}, Eq. (20) involves the evaluation of c_f^a and, therefore, of the double integral in Eq. (16). By virtue of the previous assumptions (a)-(d), the c_f^a coefficient becomes:

$$c_f^a = \left(\frac{\rho c_{ls,ref}^{rms} b_{ref}^2}{16\, m_j St^2}\right)^2 \frac{n_j}{\pi^3} S_{ss}^*(z_{ss}; n_j)\, L^2\, \mathscr{G}_j(\kappa_s) \tag{32}$$

with:

$$S_{ss}^*(z_{ss}; n_j) = \frac{1}{\sqrt{\pi} B(z_{ss}) n_j} \tag{33}$$

$$\mathscr{G}_j(\kappa_s) = \int_0^1 \int_0^1 \psi_j(\zeta)\, \psi_j(\zeta')\, \exp\{-\kappa_s|\zeta - \zeta'|\} d\zeta\, d\zeta' \tag{34}$$

where the spectral density function is herein described by the Vickery and Clark expression (Vickery and Clark, 1972), B being the bandwidth spectral parameter, e.g., $B(z) = \sqrt{0.08^2 + 2I_u^2(z)}$. The coherence function has been expressed by an exponential function, which is often used in the literature (e.g., ESDU 96030, 1998; Piccardo and Solari, 2000); $\zeta = z / L$ is a dimensionless coordinate, $\kappa_s = \lambda/\mathscr{L}$ with $\mathscr{L}$ the correlation length (in b_{ref}) and $\lambda = L/b_{ref}$ the structural slenderness.

Including the developments described above and picking out the terms with the purpose of comparing the relevant formulae with those in codes and guidelines, c_{2F} can be re-written in the form:

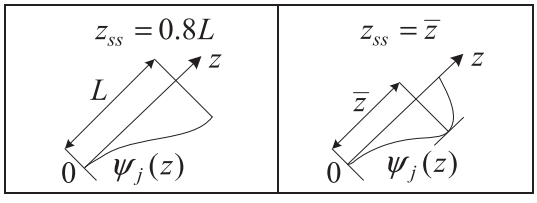

Fig. 5. Examples of estimation criterion for the VIV reference coordinate z_{ss}.

$$c_{2F} = \frac{\rho b_{ref}^2}{m_{ej}} \frac{a_L^2}{c_1^a} \frac{C_c^2}{St^4} \frac{b_{ref}}{L} \tag{35}$$

being:

$$C_c = \frac{\sqrt[4]{\pi} c_{ls,ref}^{rms}}{2^4 \pi^2} \frac{1}{\sqrt{B(z_{ss})}} \mu_c \tag{36}$$

$$\mu_c = \frac{\sqrt{\lambda\, \mathscr{G}_j(\kappa_s)}}{I_j} \tag{37}$$

$$I_j = \int_0^1 \psi_j^2(\zeta) d\zeta \tag{38}$$

where C_c is the so-called aerodynamic coefficient and μ_c is a structural correction factor accounting for partial correlation in space and depending on slenderness and modal shape.

The closed-form solution of the function $\mathscr{G}_j$, then of μ_c, for various modal shapes of structural interest is now investigated. Appendix A reports the exact solution, together with the value of I_j. Table 1 summarizes the results reporting the correction factor μ_c for different slenderness values, considering $\kappa_s = \lambda$, i.e. $\mathscr{L} = 1$ (i.e., correlation length equal to one diameter, value commonly used in generic situations). Besides a slight dependence on λ, that becomes evanescent as λ grows enough, Table 1 highlights large differences between the μ_c values related to different mode shapes. In the following Section, $\lambda = 30$ is chosen as the basic case for comparative studies.

Hansen (2007) proposed a similar formulation of the aerodynamic coefficient C_c that is modulated by a correction factor γ_c. Comparing it with Eq. (36), it is possible to verify that γ_c and μ_c are linked through the relationship $\gamma_c = \mu_c/\sqrt{2}$. However, γ_c accounts for the modal shape only and its calculation involves line integrals of the spectral function and mode shape. The solution is provided by the author for five common modal shapes (i.e., $\psi_j(\zeta) = 1,\ \zeta,\ \zeta^2,\ \sin(\pi\zeta),\ 2\zeta - 1$; see Table 1 in Hansen, 2007). For λ>20, the estimates of γ_c for the cited five modal shapes lead to values that differ of about +5% from the corresponding structural correction factor μ_c provided here. Differences can be higher at smaller λ.

The solution becomes even simpler for the class of the common modal shapes that do not change sign. In this case, the EST allows expressing the function $\mathscr{G}_j$ in closed form (Piccardo and Solari, 1998):

$$\mathscr{G}_j = \mathscr{C}(\kappa_s \cdot k_{sj}) \left[\int_0^1 \psi_j(\zeta) d\zeta\right]^2 \tag{39}$$

being

$$k_{sj} = \frac{1}{2}\left(\frac{1}{|\psi_j(\widehat{z})|} \int_0^1 |\psi_j(\zeta)| d\zeta\right)^{0.55} \tag{40}$$

$$\mathscr{C}\{\omega\} = \frac{1}{\omega} - \frac{1}{2\omega^2}\left(1 - e^{-2\omega}\right) \quad \text{for} \quad \omega > 0; \quad \mathscr{C}\{0\} = 1 \tag{41}$$

The following closed-form solution for μ_c is also derived:

$$\mu_c = \sqrt{\lambda\ \mathscr{C}\left[k_{sj} \cdot \frac{\lambda}{\mathscr{L}}\right]}\ I_{sj} \tag{42}$$

$$I_{sj} = \frac{\int_0^1 \psi_j(\zeta) d\zeta}{\int_0^1 \psi_j^2(\zeta) d\zeta} \tag{43}$$

In order to check the accuracy of this approximate solution, symbols in Fig. 6 represent the quantity $\mathscr{G}_j$ obtained by the closed-form expression, combining Eqs. (37) and (42), for a selection of common mode

Table 1
Values of μc for different slenderness and modal shapes ($\mathscr{L}$=1).

λ	$\psi_j(\zeta)$								
	1	$\sin(\pi\zeta)$	$\sin\left(\frac{\pi\zeta}{2}\right)$	$\frac{[1-\cos(2\pi\zeta)]}{2}$	ζ	ζ^2	$(2\zeta-1)$	$\sin(2\pi\zeta)$	$\sin\left(\pi\zeta+\frac{\pi}{2}\right)$
10	1.342	1.925	1.879	2.191	2.262	2.798	2.067	1.741	1.726
20	1.378	1.978	1.944	2.274	2.356	2.972	2.260	1.917	1.877
30	1.390	1.990	1.964	2.293	2.388	3.034	2.324	1.960	1.922
40	1.396	1.994	1.973	2.300	2.403	3.065	2.356	1.977	1.944
50	1.400	1.996	1.979	2.303	2.412	3.084	2.375	1.985	1.956

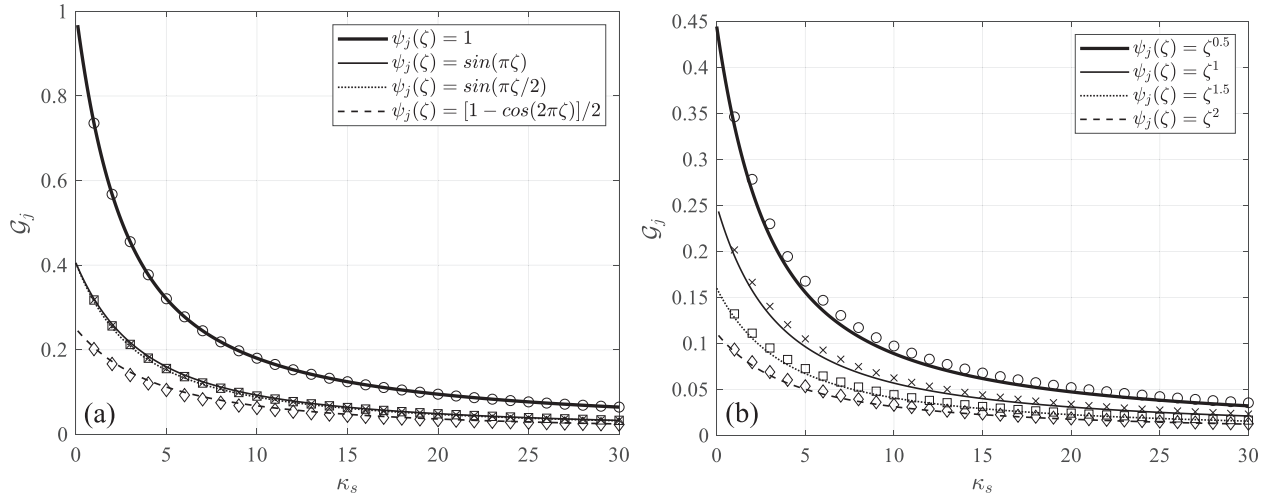

Fig. 6. Approximate closed-form (symbols) and exact (lines) solution of $\mathscr{G}_j$ for a selection of common mode shapes without change of sign: constant and sinusoidal (a), cantilever (b).

shapes; solid lines represent the exact solution of the integral (34) (see Appendix A). The agreement is excellent confirming the validity of the proposed approach. Table 2 reports the quantities k_{sj} and I_{sj}.

Table 3 summarizes the sequential steps necessary to determine the VIV coefficients according to the procedures proposed in this paper. A crucial step is represented by the evaluation of the correction factor μ_c, which can be estimated for any modal form (Step 6a) or in closed form for modal shapes not changing in sign (Step 6b). Therefore, the reader can derive simple calculation schemes for any case of specific interest.

5. Numerical discussion

This Section discusses the application of the proposed solutions investigating the relevant quantities involved and the possible errors committed concerning circular cross-section cylinders. The comparison with European guidelines shows possible criticisms in code provisions and highlights the effectiveness of the proposed developments. The incompleteness of data precludes in-depth analyses for non-circular cylinders.

Section 5.1 carries out parametrical analyses, investigating the role of structural properties and flow conditions. Starting from the parameters previously defined, Section 5.2 investigates the VIV domain limits from both the qualitative and quantitative point of view. Section 5.3 studies a real chimney that was the object of extensive full-scale experiments. Using the outcomes of the proposed solution, the estimate of VIV amplitude is carried out at different approximation levels. It is emphasized that the greatest interest of the work is on the "forced vibration" regime since a revision of the limiting amplitude a_L (which govern the "lock-in" regime) is not addressed in this context.

5.1. Discussion on model parameters

This Section considers a circular cylinder characterized by a reference choice of the model parameters. The objective is to investigate from a quantitative point of view, through suitable ranges of Scruton number, the regime domains characterizing VIV response (Section 3).

The slenderness is set as $\lambda = 30$, that represents the average value of most chimneys investigated in the literature (e.g., the data survey reported by Lupi et al., 2017), and of the measures gathered by CNR (2008) for the peak coefficient assessment (see Pagnini and Piccardo, 2017). According to a prudential choice usually assumed by codes, the analysis first considers smooth flow conditions, i.e. $I_u = 0$. The r.m.s. lift coefficient is described according to ESDU 96030 (1998); it depends on *Re* and on the surface roughness ε (Fig. 7).

Considering a selection of non-changing sign modal shapes that are representative of common structural typologies, diagrams in Fig. 8 show the quantity C_c provided by Eq. (36) for dimensionless surface roughness $\varepsilon/b = 0.1\ 10^{-3}$ (Fig. 8a), which is representative of a steel painted surface, and for $\varepsilon/b = 0.5\ 10^{-3}$ (Fig. 8b), representative of rusty surface. It is apparent that the surface roughness greatly affects the numerical value of C_c that maintains the trend of the r.m.s. lift coefficient. Therefore, at high

Table 2
Values of k_{sj}, I_{sj} useful for closed-form calculations for different modal shapes without change of sign.

$\psi_j(\zeta)$	1	$\sin(\pi\zeta)$	$\sin(\pi\zeta/2)$	$[1-\cos(2\pi\zeta)]/2$	$\zeta^{0.5}$	ζ	$\zeta^{1.5}$	ζ^2
k_{sj}	0.5	0.390	0.390	0.342	0.400	0.342	0.302	0.273
I_{sj}	1	$4/\pi$	$4/\pi$	4/3	4/3	3/2	8/5	5/3

Table 3
Sequential steps to determine VIV coefficients.

Step	Operations
1	Assign L, b_{ref},
2	Assign ρ, n_j,ξ_j, $\mu(z)$, $\psi_j(z)$; calculate m_j, m_{ej}, Eq. (10), and Sc
3	Assume z_{ss} (e.g., Fig. 5); at z_{ss} calculate St and Re_{ss} (if necessary, in iterative manner; e.g., CNR, 2008)
4	Assign $I_u(z_{ss})$ and calculate K_{a0} (from I_u and Re_{ss}; e.g., Hansen, 2007; Pagnini and Piccardo, 2017), then $c_1^a = K_{a0}$
5	Determine $\psi_j(\widehat{z})$, assign κ, calculate $a_L = 1/\kappa\psi_j(\widehat{z})$ and c_{1F}, Eq. (31)
6a *for any modal shape*	Calculate $\lambda = L/b_{ref}$, assign $\mathscr{L}$, calculate $\kappa_s = \lambda/\mathscr{L}$, I_j (Eq. (38)) and the function $\mathscr{G}_j$ from Eq. (34) or Appendix A (for a selection of modal shapes of common use); finally determine μ_c from Eq. (37)
6b *for modal shapes not changing in sign*	Calculate k_{sj} from Eq. (40) or from Table 2, calculate $\lambda = L/b_{ref}$, assign $\mathscr{L}$, calculate $\mathscr{C}(k_{sj}\cdot\lambda/\mathscr{L})$ from Eq. (41) and I_{sj} from Eq. (43) or Table 2; finally determine μ_c from Eq. (42)
7	Assign the surface roughness ε, estimate $c_{ls,ref}^{rms}$ (e.g., ESDU 96030, 1998 or next Fig. 7, from Re_{ss} and ε/b_{ref}), assign B (z_{ss}) (e.g., $B = \sqrt{0.08^2 + 2I_v^2(z_{ss})}$), calculate C_c, Eq. (36)
8	Calculate c_{2F}, Eq. (35)
9	Compare Sc with the domain limits $4\pi c_1^a(1 \pm 2\sqrt{5}\sqrt{c_{2F}}/a_L^2)$ as in Eqs. (27), (28) and determine the VIV regime. Accordingly, calculate $\tilde{\sigma}_{aj}$ either by Eq. (27), (28), or Eq. (18)

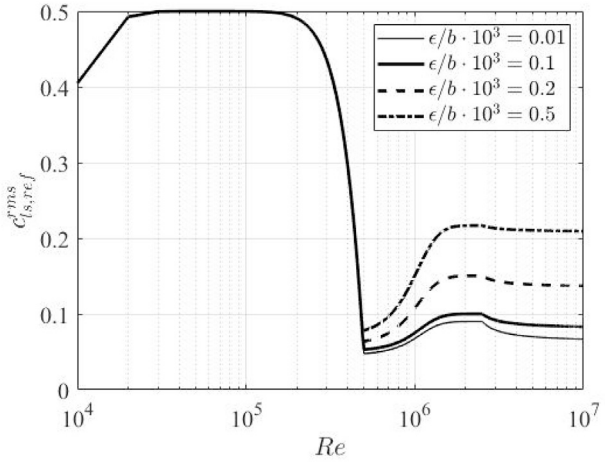

Fig. 7. R.m.s. lift coefficient, reworking by ESDU 96030 (1998).

Reynolds number, an inaccurate assessment of the surface finishing may result in significant errors in its estimation. These figures also reveal the large influence of the mode shape. Estimates provided by the codes, reported by grayscale lines, only depend on Re; they lie quite below the results of Eq. (36) at low Reynolds numbers (i.e., $Re < 5{\cdot}10^5$), while, at high Reynolds numbers, they supply an average upper bound at low roughness conditions, i.e. for well-maintained painted steel structures, and an average lower bound at high roughness conditions. Then, in smooth flow conditions, code prescriptions seem rather inaccurate and appear conservative for smooth surfaces at sufficiently high Reynolds number only.

Referring to $\varepsilon/b \leq 0.1\ 10^{-3}$, Fig. 9 investigates the role of turbulence intensity, showing that the information given by code prescriptions is now completely different. Even for small values of I_u (e.g., $I_u = 0.1$), the codes considered provide large overestimates for $Re > 5\ 10^5$, whereas they are in line with average values of C_c for low Re values. Neglecting the dependence on the mode shape and the turbulence intensity in the evaluation of the aerodynamic constant C_c seems to be a serious lack of code prescriptions.

The mass ratio acts in the opposite way of λ. Its growth slightly increases the forced domain lower bound and enlarges the transition range. It is assumed $\rho b_{ref}^2/m_{ej} = 0.01$, which represents an average value of chimney collections found in the literature (e.g., Lupi et al., 2017).

The value of the limiting amplitude a_L needs to be set for estimating the VIV domain limits, Eq. (29). According to the mentioned codes, $a_L = 0.4$, that corresponds to a maximum dimensionless displacement greater than 0.57. To the authors' knowledge, however, there are no measurement reports that justify this choice. Consistently with the values measured on chimneys and other circular cylinders excited by the wind (e.g., Clobes et al., 2012; Lupi et al., 2017) $a_L = 0.2$ seems a suitable choice (consistent with the maximum measured amplitudes) and it is assumed as a reference value in the following. In-depth studies on this parameter are outside the scope of this work.

Within the approximate framework of Section 4, the parameter c_1^a is completely defined by K_{a0}, Eq. (30). In the following, St and K_{a0} are deduced by EN 1991-1-4 (2005): the former is set to 0.18, the latter is assigned as a function of the Reynolds number, i.e., $K_{a0} = 2$ for $Re \leq 10^5$, $K_{a0} = 0.5$ for $Re = 5{\cdot}10^5$, $K_{a0} = 1$ for $Re \geq 10^6$, assuming a linear variation with $\log_{10}(Re)$ for intermediate values. Such K_{a0} values are referred to $I_u = 0$, leading to conservative predictions of VIV response. The influence of turbulence will be considered in the sequel.

5.2. Evaluation of VIV domain limits

With the assumptions previously discussed, VIV regimes are completely defined according to Section 3. A qualitative study of the limit domains is possible at least in the ideal case of laminar, uniform free-stream conditions, i.e. $I_u = 0$. Through Eqs. (20) and (35), the VIV domain limits (29) can be expressed as:

$$4\pi c_1^a\left(1 - \frac{2\sqrt{5}}{a_L}\sqrt{\frac{1}{c_1^a}\frac{\rho b_{ref}^2}{m_{ej}}\frac{C_c^2}{St^4}\frac{1}{\lambda}}\right) < Sc < 4\pi c_1^a\left(1 + \frac{2\sqrt{5}}{a_L}\sqrt{\frac{1}{c_1^a}\frac{\rho b_{ref}^2}{m_{ej}}\frac{C_c^2}{St^4}\frac{1}{\lambda}}\right) \tag{44}$$

It is therefore clear, in analogy to C_c values, that the domain limits are governed by Reynolds number. Using reference values discussed in the previous Section 5.1 and noting that the largest C_c values occur for $\psi_j(\zeta) = \zeta^2$, i.e. $C_c \cong 0.046$ for $\mathrm{Re} \leq 2{\cdot}10^5$ and $C_c \cong 0.0092$ for $\mathrm{Re} \geq 2{\cdot}10^5$ and $\varepsilon/b = 0.1\ 10^{-3}$, Eq. (44) can be rewritten as:

$$\begin{aligned} &8\pi\left(1 - \frac{0.0820}{a_L}\right) < Sc < 8\pi\left(1 + \frac{0.0820}{a_L}\right) \quad for \quad Re \leq 2\cdot 10^5 \\ &4\pi\left(1 - \frac{0.0232}{a_L}\right) < Sc < 8\pi\left(1 + \frac{0.0232}{a_L}\right) \quad for \quad Re \geq 5\cdot 10^5 \end{aligned} \tag{45}$$

Therefore, the largest possible extension of the "transition" regime obtainable for $a_L = 0.2$ can be roughly quantified in:

$$\begin{aligned} &Sc \in [8\pi(1 \pm 0.41)] \quad for \quad Re \leq 2\cdot 10^5 \\ &Sc \in [4\pi(1 \pm 0.12)] \quad for \quad Re \geq 5\cdot 10^5 \end{aligned} \tag{46}$$

Using $a_L = 0.4$, as suggested by codes and literature (e.g., EN 1991-1-4, 2005; Verboom and van Koten, 2010), the values in Eq. (44) are halved, i.e. (1 ± 0.205) and (1 ± 0.06). Therefore, the use of the value $a_L = 0.2$ also appears to be more conservative (as well as more realistic, as previously discussed) postponing the onset of the "forced vibration" regime.

Eq. (46) provides a first qualitative estimate, strongly conservative, of the application validity of the VIV approximate solutions $\tilde{\sigma}_{aj}^f$ and $\tilde{\sigma}_{aj}^{nl}$. Focusing in particular on $\tilde{\sigma}_{aj}^f$, it allows setting the following conditions for the forced VIVs: $Sc > 35$, if $Re \leq 2{\cdot}10^5$ and $Sc > 14$, if $Re \geq 2{\cdot}10^5$ (assuming $a_L = 0.2$). With respect to the Scruton numbers suggested by codes, these values greatly expand the forced domain; moreover, they can be further reduced considering the effect of longitudinal turbulence and different modal shapes, as will be highlighted by the following

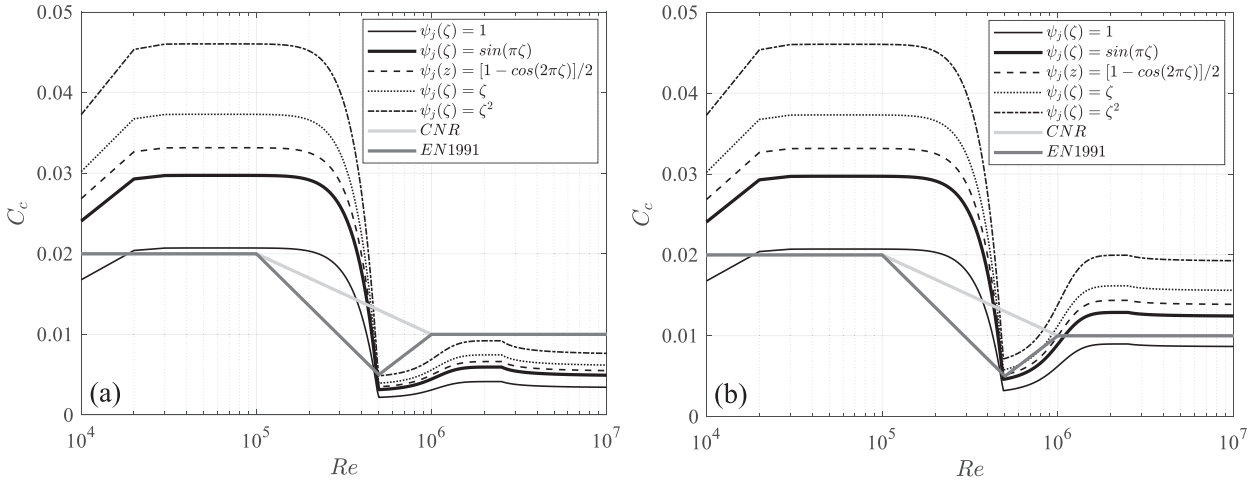

Fig. 8. Parametric diagrams of the aerodynamic constant C_c; $\lambda = 30$, $I_u = 0$, $\varepsilon/b = 0.1\ 10^{-3}$ (a), $\varepsilon/b = 0.5\ 10^{-3}$ (b).

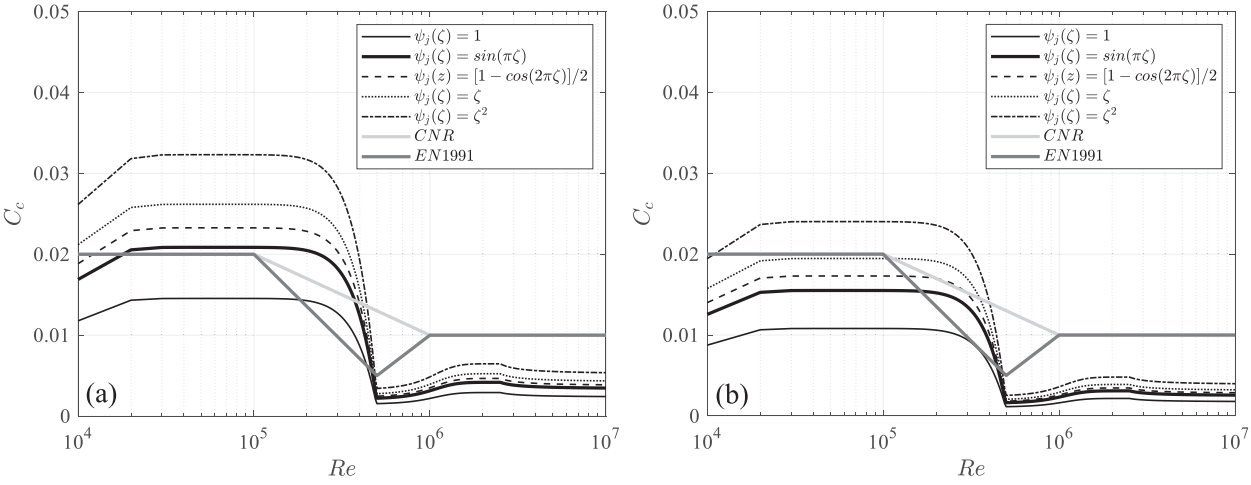

Fig. 9. Parametric diagrams of the aerodynamic constant C_c; $\lambda = 30$, $\varepsilon/b = 0.1\ 10^{-3}$, $I_u = 0.1$ (a), $I_u = 0.2$ (b).

numerical examples. The surface finish can influence these results leading to a reduction of the validity domain of the forced solution in the presence of high roughness (e.g., rusty surface).

Fig. 10 a-d show the limit values of *Sc* for the application of the approximate forced and lock-in solution, Eqs. (27), (28), depicted by thin and thick solid line, respectively, for various modal shapes, concerning laminar, uniform free-stream conditions. The dashed line in the diagrams reports the reference value $Sc = 4\pi K_{a0}$. It represents the usual discriminating value between the two different regimes.

Major evidences concern the large variations with *Re* of the limit boundaries, their change similar to $4\pi K_{a0}$ behavior and the narrowing of the transition domain around $4\pi K_{a0}$. Such trend is mainly related to the variation of K_{a0} with *Re* and involves the activation of the lock-in regime at lower *Sc* values as *Re* increases. This behavior suggests that the "forced vibration" and "lock-in" regimes are not defined by fixed values of *Sc*. In particular, in the absence of turbulence, the limit value $Sc = 30$, that some codes suggest to reduce the risk of synchronized oscillations (e.g., CNR, 2008), is suited for low *Re* (less than 10^5), whereas it is largely overestimated for $Re > 5 \times 10^5$, where a Scruton number threshold of about 15 is enough to lie in the "forced vibration" regime. A constant limit value is hard to be established in the intermediate domain; following the r.m.s. lift coefficient, it is very sensitive to *Re* variation; however, for trans-critical and super-critical Reynolds number, the forced regime is always associated with lower (or much lower) values of *Sc* compared to the sub-critical case.

The presence of turbulent conditions is then investigated modulating the aerodynamic damping parameter K_{a0} by the correction factor K_v proposed by Hansen (2007), i.e. $K_v = 1–3 \cdot I_u$ for $I_u < 0.25$ and $K_v = 0.25$ for $I_u \geq 0.25$. Assuming $\psi(\zeta) = \zeta^2$, that is the typical first mode of many chimneys (and provides the highest *Sc* values for the occurrence of the "forced vibration" regime), Fig. 11 considers $I_u = 10\%$ (Fig. 11 a) and $I_u = 20\%$ (Fig. 11 b). The application in turbulent regime leads to a marked reduction of the reference value $4\pi K_{a0}$ and, then, of the *Sc* limits. Similar trends can be observed for other modal shapes. In particular, the limit curve that describes the forced domain in terms of *Sc* undergoes notable decrease up to be less than $Sc = 30$ for any Reynolds number; in particular, it becomes less than 10 for turbulence intensity equal to 0.1 and less than 6 for $I_u = 0.2$ at $\mathrm{Re} > 3–4 \times 10^5$, i.e. in trans-critical and super-critical regime.

Moreover, for the investigated circular cylinders, in the range $Re > 5 \times 10^5$, typical of real structures, independently from turbulence conditions, the boundaries of the transition domain are quite narrow, due to the small values of the coefficient c_{2F} that, in turn, is related to the decrease of C_c (as highlighted in Figs. 8 and 9). In this case, the limit values of the *Sc* defining the "forced vibration" and "lock-in" regimes are very close to the reference value $4\pi K_{a0}$, in disagreement with the conditions "*much smaller than*", "*much greater than*" usually reported in the literature (e.g., Vickery and Basu, 1983a).

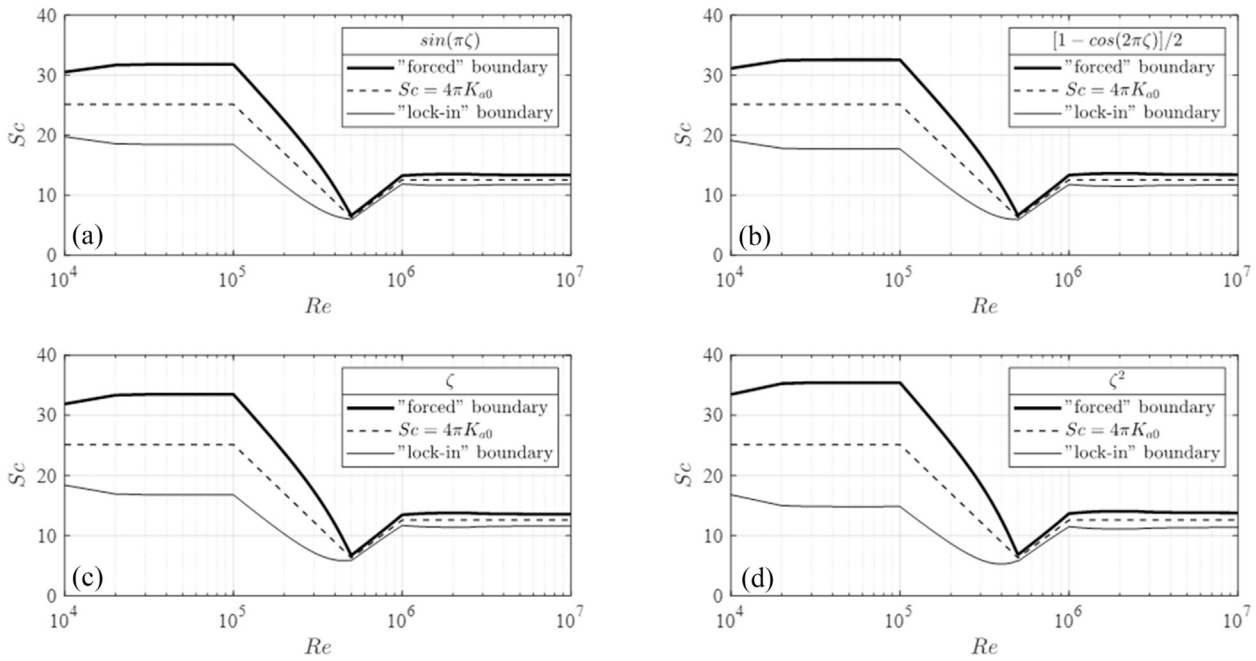

Fig. 10. Domain limits for the proposed simplified solution in forced and lock-in regime; test case assuming $\lambda = 30$, $a_L = 0.2$, $\rho b_{ref}^2/m_{ej} = 0.01$, $I_u = 0$, $\varepsilon/b \leq 0.1\ 10^{-3}$ for a selection of modal shapes.

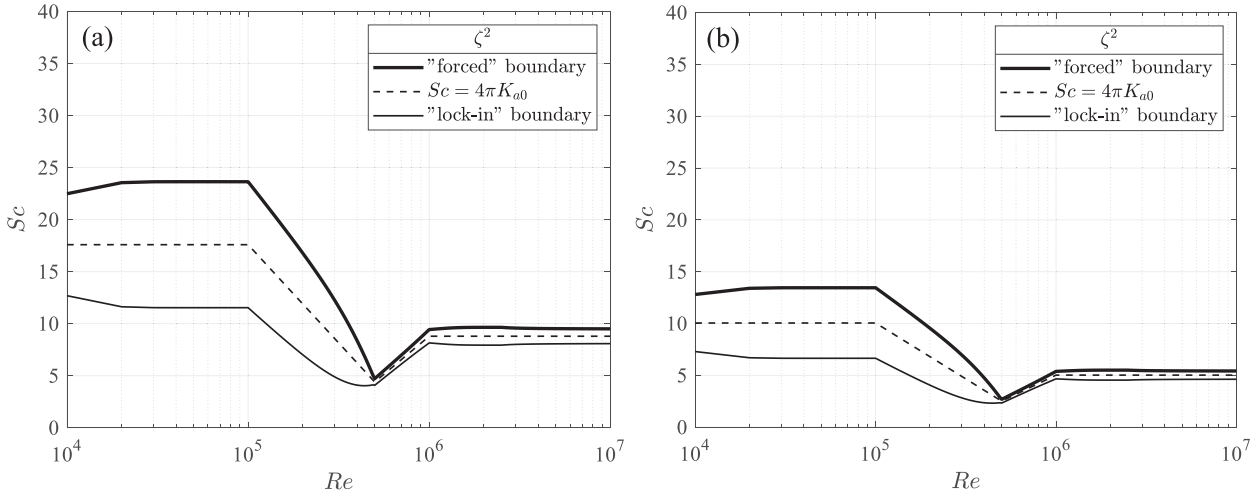

Fig. 11. Domain limits for the proposed simplified solution in forced and lock-in regime; test case assuming $\lambda = 30$, $a_L = 0.2$, $\rho b_{ref}^2/m_{ej} = 0.01$, $\psi(\zeta) = \zeta^2$, $\varepsilon/b \leq 0.1\ 10^{-3}$, $I_u = 0.1$ (a), $I_u = 0.2$ (b).

5.3. Full-scale case study

The illustrated procedure is applied to a full-scale steel chimney in Brovst (Denmark) that was instrumented and tested within a field experiment concerning cross-wind excitation of circular cylinders. The main description and results of such measurements are given by Christensen and Frandsen (1978), Frandsen (1979) and are also reported by Dyrbye and Hansen (1997) and Clobes et al. (2012). It should be noted that, in full-scale measurements, the evaluation of the maximum oscillation amplitudes presents a certain degree of uncertainty. On the other hand, accurate theoretical predictions of VIV response require a precise estimate of turbulence intensity and structural damping, which is uncertain by its nature. For all these reasons, the choice fell on an adequately documented case-study to try to limit the uncertainties inherent in the VIV prediction of actual structures, that is particularly challenging.

The structure is 54 m high with constant diameter $b = 2.2$ m, $n_1 = 0.61$ Hz, $\xi_1^m = 1\%$, $Sc = 15.9$, $S = 0.17$, $Re_{ss} = 9.83 \times 10^5$. The fundamental mode shape is assumed $\psi(\zeta) = \zeta^2$. The terrain roughness length is $z_0 = 0.05$ m, as indicated in the reference papers. Turbulence intensity is estimated by $I_u = \frac{1}{\log(z_{ss}/z_0)} \sim 15\%$. The wind profile is represented by a logarithmic law. Being characterized by rusty surface, it is supposed $\varepsilon = 1$ mm, therefore $\varepsilon/b = 0.4 \times 10^{-3}$. The source paper supplies $St = 0.2$; on the other hand, $St = 0.18$ and $St = 0.26$, according to Eurocode and CNR, respectively, with obvious consequences on the estimate of the critical wind velocity. In the face of such discrepancy, and with the purpose of comparing results based on the same choice of parameters, the calculations have been carried out using $St = 0.2$. Then, the critical condition in terms of reduced wind velocity $U/n_1 b$ can be expressed as $1/\mathrm{St} = 5$.

The information on the VIV regime are supplied by the domains given by Eqs. (27) and (28) in terms of Scruton number. Using $a_L = 0.2$, applying either Eurocode or CNR, the forced domain is described by

$Sc>\sim 14$. The lower bound becomes less restrictive when it accounts for turbulence in the estimate of K_{a0} (using the correction factor proposed in Hansen, 2007) and even more using Eqs. (35), (36) and (42). In this case, the forced domain applies for $Sc>\sim 8$. Therefore, the structural behavior is of forced type and the approximate solution $\tilde{\sigma}_{aj}^{f}$ can be applied.

The proposed solution is investigated, first, in terms of the quantity c that rules the VIV response, Eq. (15), that depends on c_f^a, Eq. (32), and that, therefore, can be calculated through the analytical procedure proposed in Section 4. Fig. 12 shows the value obtained with the full integral solution supplied by Eq. (16), versus the reduced wind velocity at the top, and by the proposed closed-form solution. Since the simplified solution assumes the critical VIV onset at z_{ss}, the corresponding reduced wind velocity at the top is slightly higher than 1/St. It is also observed that the full integral solution has its maximum value for a little higher wind speed; evidently, in this case the critical velocity of maximum VIV occurs at a position $z_{ss}<0.8L$, so that the wake excitation is spread over a larger portion around z_{ss} (e.g., Verboom and van Koten, 2010). Such maximum value is a little lower than the proposed closed-form solution, that provides a prudential overestimate of about 5%.

The comparison with experimental measures, that are supplied in terms of maximum response, requires the evaluation of the peak factor. It is about $\sqrt{2}$ for deterministic harmonic oscillations at very small Scruton numbers. It is about 4 at large Scruton numbers, when the response is random Gaussian and narrow banded. Available formulations are very uncertain elsewhere. It is assumed about 2.9 for the following case study, in agreement with CNR (2008), which proposes an improvement over the common assessments (Pagnini and Piccardo, 2017). Further investigation on this topic, which goes beyond the interest of this paper, are addressed by Chen (2014).

The solid line in Fig. 13 shows the standard deviation of the structural response obtained by the full numerical solution, Eq. (18), on varying the reduced wind velocity; the dashed line represents the value derived from the measured maximum (the measured wind speed is not reported in the reference document) that reveals a sound agreement with the estimate. Gray filled symbols represent the values obtained by CNR and Eurocode evaluations, that consider the critical VIV onset at the top, i.e., $z_{ss}=L$ (maximum point of the eigenvector). At this step, the reported estimates do not account for turbulence intensity, nor consider corrective factors in this regard. These outcomes result in heavy overestimates that can be mitigated with the following developments.

The estimate of the aerodynamic damping parameter K_{a0} can be reduced accounting for turbulence effect on the vortex shedding phenomenon. The CNR guideline supplies a specific relationship that leads to a slight improvement of the previous estimate (white circle in Fig. 13),

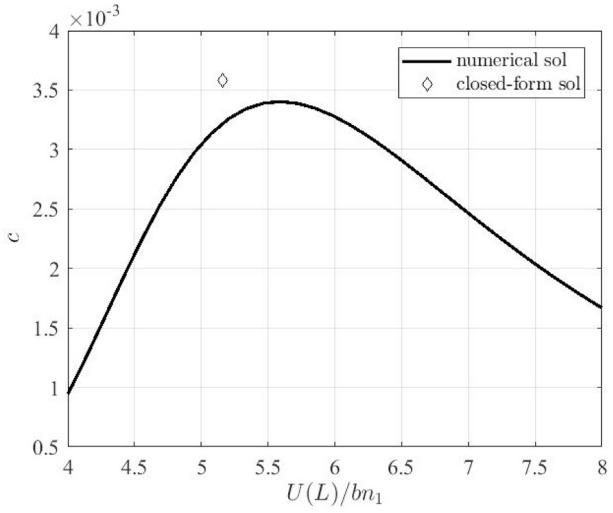

Fig. 12. Aerodynamic coefficient c of the Brovst chimney.

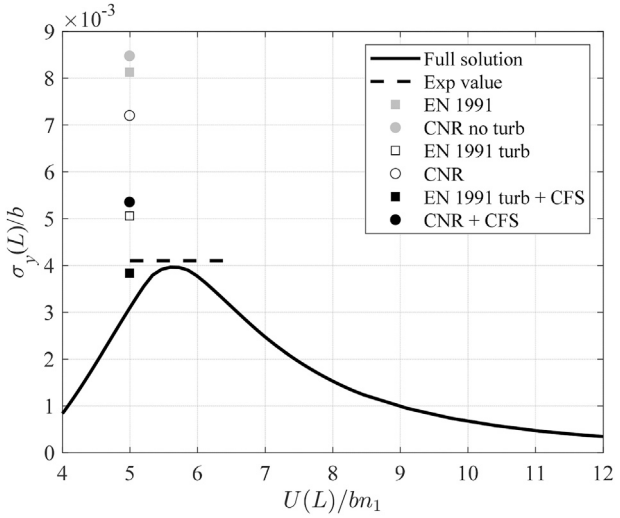

Fig. 13. Structural response of the Brovst chimney (CFS = closed-form solution).

but seems still unsuitable to adequately reproduce the actual behavior. Eurocode does not supply any procedure for this purpose and refers to the National Annexes for possible corrections. Using the correction factor proposed in Hansen (2007), the new estimate (white square in Fig. 13) comes closer to the measured value, although it is about 30% higher.

The code provisions are then applied using the expression of the aerodynamic coefficient derived in the framework of the proposed closed-form solution, Eqs. (36) and (42), maintaining the turbulence correction of K_{a0} used in the previous step. The solution further approaches the measure (black filled symbols in Fig. 13). In particular, for this case study, the evaluation by Eurocode is very close to the full solution and to the experimental measure. This last result highlights the potential of the proposed procedure, which can easily be embedded in a technical context.

6. Concluding remarks and prospects

Most of the technical regulations on wind-excited structures adopt the spectral phenomenological model for the calculation of vortex-induced response. However, the expressions supplied at this regard are usually poorly detailed; for instance, current European Codes are lacking in prescriptions for a correct evaluation of the aerodynamic coefficient governing VIV also for the circular cross-section. They take into account the dependence on Reynolds number but ignore a number of factors that can greatly modified its evaluation.

The outcomes of the spectral model can be considered reliable in the "forced vibration" regime, when the structural damping is sufficiently greater than the aerodynamic damping. They turn out to be quite or very uncertain both in the "lock-in" regime, when the structure can exhibit large crosswind vibrations, and in the "transition" regime, where the situation is intermediate between the two border cases. The spectral model is not specifically calibrated to work in these domains, as expressly stated by Basu and Vickery (1983), even though it has often been used precisely for estimates of lock-in vibrations. In these conditions, its application can lead to very conservative results, often quite far from the real behavior of the structure. On the other hand, to the best of authors' knowledge, the boundaries of the various regimes have never been defined quantitatively in the scientific literature. For this reason, using a simple and expressive parameter such as the Scruton number, it is not easy to define a priori the actual sensitivity of a structure towards the VIV phenomenon.

The present paper fills this gap proposing the quantitative assessment of the domains where the VIV assumes different characteristics as a

function of the same parameters governing the response amplitude. In this way, it is possible either to exclude the "lock-in" and "transition" regime or to consider their onset. Within the limit domains of "forced vibration" and "lock-in" regime, simplified formulations for VIV calculations can be used. The a priori knowledge of the response domain appears extremely important during both the design and the verification phase. From one hand, it is possible to use this information to evaluate the possibilities of designing a structure in "forced vibration" regime. On the other hand, the knowledge of the behavior regime provides sensitivity to the uncertainty of the VIV calculations.

It seems appropriate to clarify that the "forced vibration" regime is at present identified according to qualitative empirical criteria. For example, regarding the circular section, CNR (2008) writes that "if the Scruton number is greater than 30, the risk of synchronization is very reduced". In light of the results of this paper, this limit is reasonable for small Reynolds numbers only, i.e. $Re < 1–2{\cdot}10^5$, in a sub-critical regime and in complete absence of turbulence. Outside these values, the "forced vibration" regime onset broadens greatly and the "transition" regime becomes extremely narrow. At $Re \geq 5{\cdot}10^5$, that represents a very common case in engineering practice, a Scruton number greater than 14 ensures forced conditions in the absence of turbulence, decreasing to less than 10 with $I_u = 10\%$.

Moreover, with regard to the "forced vibration" regime, this paper discusses the choice of the model parameters and the uncertainties connected, supplying new analytical developments aimed at the engineering application of the procedure. With the support of numerical results, the remarkable importance of the mode shape (neglected by the main European codes) on the calculation of the VIV response is highlighted; also the surface roughness can significantly influence the response in the super-critical regime of Reynolds numbers. Concerning mode shapes without change of sign, a closed-form derivation of the force coefficient is proposed fully coherent with main national and European regulations. This relationship is therefore perfectly suitable for use in structural calculations carried out in compliance with the current standards.

Within a spectral approach for the evaluation of the VIV response, the considerations made in this paper can also be used for the "transition" and "lock-in" regimes and the for calculation of the maximum response (e.g., Pagnini, 2017). However, as previously mentioned and widely discussed in Pagnini and Piccardo (2017), a reliable calculation in these regimes cannot leave out of consideration an adequate discussion of the limiting amplitude. As far as the maximum response is concerned, a technical review of the peak coefficient in the "transition" regime seems to be appropriate.

The proposed formulation is suitable for cylinders with any cross-section. All the applications dealt with in this paper, however, are restricted to circular cylinders. The incompleteness of data (e.g., concerning the K_{a0} coefficient) precludes similar in-depth analyses for non-circular cylinders, such as square and rectangular shaped structures. The analyses developed in this paper may represent a useful pattern and reference point, when such data become available.

Finally, it is worth noting that the matter discussed in this paper is classically implicitly addressed to synoptic wind conditions producing stationary VIVs. The advanced procedure proposed herein in terms of simplifications and clarifications of this complex phenomena represent a fundamental starting point to generalize their treatment to the transient conditions involved by the sudden gust fronts due to thunderstorm outflows (e.g., Solari et al., 2015a; Solari et al., 2015b; Le and Caracoglia, 2016; Solari, 2016).

Declaration of competing interest

The authors declare that they have no known competing financial interests or personal relationships that could have appeared to influence the work reported in this paper.

CRediT authorship contribution statement

L.C. Pagnini: Methodology, Resources, Software, Validation, Writing - original draft, Writing - review & editing. **G. Piccardo:** Conceptualization, Methodology, Software, Visualization, Writing - original draft, Supervision. **G. Solari:** Writing - review & editing, Funding acquisition.

Acknowledgements

This research is funded by the European Research Council (ERC) under the European Union's Horizon 2020 research and innovation program (grant agreement No. 741273) for the project THUNDERR - Detection, simulation, modelling and loading of thunderstorm outflows to design wind-safer and cost-efficient structures – supported by an Advanced Grant 2016.

Appendix A. Supplementary data

Supplementary data to this article can be found online at https://doi.org/10.1016/j.jweia.2020.104100.

References

Acebedo, R., Kim, S.-W., Hwang, Y.-C., Kim, H.-K., 2016. Effect of turbulence length scale on vortex induced vibration of twin deck bridge section. In: Proc. Advances in Civil, Environmental and Materials Research, ACEM16, Korea.
Basu, R.I., Vickery, B.J., 1983. Across-wind vibrations of structure of circular cross-section. Part II. Development of a mathematical model for full-scale application. J. Wind Eng. Ind. Aerodyn. 12 (1), 75–97.
Blevins, R.D., 2001. Flow-induced Vibration, second ed. Krieger Publ Company, Malabar FL.
Chen, X., 2014. Extreme value distribution and peak factor of crosswind response of flexible structures with nonlinear aeroelastic effect. J. Struct. Eng. ASCE 140 (12), 04014091.
Christensen, O., Frandsen, S., 1978. A field study of cross wind excitation of steel chimneys. In: Holand, I., Kavlie, D., Moe, G., Sigbjörnsson, R. (Eds.), Safety of Struct under Dyn Loading, vol 2. Tapir Publ, Trondheim, pp. 689–697.
Clobes, M., Willecke, A., Peil, U., 2012. Vortex excitation of steel chimneys: two ultimate limit states. Bauingenieur 87, S3–S8 (in German).
CNR, 2008. Guide for the Assessment of Wind Actions and Effects on Structures - CNR-DT 207/2008. National Research Council of Italy, Rome.
Daniels, S.J., Castro, I.P., Xie, Z.-T., 2016. Numerical analysis of freestream turbulence effects on the vortex-induced vibrations of a rectangular cylinder. J. Wind Eng. Ind. Aerodyn. 153, 13–25.
Dyrbye, C., Hansen, S.O., 1997. Wind Loads on Structures. Wiley, New York.
EN 1991-1-4, 2005. Eurocode 1: Actions on Structures – Part 1.4: General Actions – Wind Actions. CEN, European Committee for Standardization, Brussels (corrigendum 2010).
ESDU 96030, 1998. Response of Structures to Vortex Shedding. Structures of Circular or Polygonal Cross Section. Engineering Science Data Unit, London.
Facchinetti, M.L., de Langre, E., Biolley, F., 2004. Coupling of structure and wake oscillators in vortex-induced vibrations. J. Fluids Struct. 19, 123–140.
Farshidianfar, A., Zanganeh, H., 2010. A modified wake oscillator model for vortex-induced vibration of circular cylinder for a wide range of mass-damping ratio. J. Fluids Struct. 26, 430–441.
Frandsen, S., 1979. RISØ Kontraktrapport: Tværsvingninger Af Stålskorstene. Felmålinger, Roskilde (in Danish).
Goswami, I., Scanlan, R.H., Jones, N.P., 1993. Vortex-induced vibration of circular cylinders. II: new model. J. Eng. Mech. ASCE 119 (11), 2288–2302.
Hansen, S.O., 1999. Vortex induced vibrations of line-like structures. CICIND Rep. 15 (1).
Hansen, S.O., 2007. Vortex-induced vibrations of structures. In: Structural Engineers World Congress. Bangalore.
Hartlen, R.T., Currie, I.G., 1970. Lift-oscillator model of vortex-induced vibration. J. Eng. Mech. Div. ASCE 96, 577–591.
Holmes, J.D., 1998. Response of cylindrical structures to vortex shedding in the natural wind. In: Thompson, M.C., Hourigan, K. (Eds.), Proc. 13th Australasian Fluid Mechanics Conf., Melbourne, pp. 401–404.
Kawecki, J., Żurański, J.A., 2007. Cross-wind vibrations of steel chimneys – a new case history. J. Wind Eng. Ind. Aerodyn. 95, 1166–1175.
Le, T.-H., Caracoglia, L., 2016. Modeling vortex-shedding effects for the stochastic response of tall buildings in non-synoptic winds. J. Fluids Struct. 61, 461–491.
Lupi, F., Niemann, H.-J., Höffer, R., 2017. A novel spectral method for cross-wind vibrations: application to 27 full-scale chimneys. J. Wind Eng. Ind. Aerodyn. 171, 353–365.
Pagnini, L.C., 2017. A numerical approach for the evaluation of wind-induced effects on inclined, slender structural elements. Eur. J. Environ. Civ. En. 21, 854–873.
Pagnini, L.C., Piccardo, G., 2017. A generalized gust factor technique for evaluating the wind–induced response of aeroelastic structures sensitive to vortex induced vibrations. J. Fluids Struct. 70, 181–200.

Païdouissis, M.P., Price, S.J., de Langre, E., 2011. Fluid-structure Interactions – Cross-Flow Induced Instabilities. Cambridge Univ Press, New York.
Piccardo, G., Solari, G., 1996. A refined model for calculating 3-D equivalent static wind forces on structures. J. Wind Eng. Ind. Aerodyn. 65, 21–30.
Piccardo, G., Solari, G., 1998. Generalized equivalent spectrum technique. Wind Struct. 1, 161–174.
Piccardo, G., Solari, G., 2000. 3D wind-excited response of slender structures: closed-form solution. J. Struct. Eng. ASCE 126 (8), 936–943.
Ruscheweyh, H., 1994. Vortex excited vibrations. In: Sockel, H. (Ed.), Wind-Excited Vibrations of Structures. Springer-Verlag, Wien, pp. 51–84.
Ruscheweyh, H., Sedlaceck, G., 1988. Crosswind vibrations of steel stacks. – critical comparison between some recently proposed codes. J. Wind Eng. Ind. Aerodyn. 30, 173–183.
Scruton, C., Flint, A.R., 1964. Wind-excited oscillations of structures. Proc. Inst. Civ. Eng. 27 (4), 673–702.
Skop, R.A., Griffin, O.M., 1973. A model for the vortex-excited resonant response of bluff cylinders. J. Sound Vib. 27, 225–233.
Solari, G., 2016. Thunderstorm response spectrum technique: theory and applications. Eng. Struct. 108, 28–46.
Solari, G., 2019. Wind Science and Engineering: Origins, Developments, Fundamentals and Advancements. Springer, Switzerland.
Solari, G., Burlando, M., De Gaetano, P., Repetto, M.P., 2015a. Characteristics of thunderstorms relevant to the wind loading of structures. Wind Struct. 20, 763–791.
Solari, G., De Gaetano, P., Repetto, M.P., 2015b. Thunderstorm response spectrum: fundamentals and case study. J. Wind Eng. Ind. Aerodyn. 143, 62–77.
Tamura, Y., Matsui, G., 1979. Wake-oscillator model of vortex-induced oscillation of circular cylinder. In: Cermak, J.E. (Ed.), Proc. 5th Int Conf Wind Eng, 1085-1094. Pergamon Press, New York.
Verboom, G.K., van Koten, H., 2010. Vortex excitation: three design rules tested on 13 industrial chimneys. J. Wind Eng. Ind. Aerodyn. 98, 145–154.
Vickery, B.J., Basu, R.I., 1983a. Across-wind vibrations of structures of circular cross-section. Part I: development of a mathematical model for two-dimensional conditions. J. Wind Eng. Ind. Aerodyn. 12 (1), 49–74.
Vickery, B.J., Basu, R.I., 1983b. Simplified approaches to the evaluation of the across-wind response of chimneys. J. Wind Eng. Ind. Aerodyn. 14 (1–3), 153–166.
Vickery, B.J., Clark, A.W., 1972. Lift or across-wind response of tapered stacks. J. Struct. Div. ASCE 98 (ST1), 1–20.
Violette, R., de Langre, E., Szydlowski, J., 2010. A linear stability approach to vortex-induced vibrations and waves. J. Fluids Struct. 26, 442–466.
Wootton, L.R., 1969. The oscillations of large circular stacks in wind. Proc. Inst. Civ. Eng. 43 (4), 573–598.